Influences of material mismatch on interface crack tip field in three layered creeping materials

Yanwei Dai[1]

Institute of Electronics Packaging Technology and Reliability, Faculty of Materials and Manufacturing, Beijing University of Technology, Beijing 100124, China

Beijing Key Laboratory of Advanced Manufacturing Technology, Beijing University of Technology, Beijing 10012

ywdai@bjut.edu.cn

Fei Qin

Institute of Electronics Packaging Technology and Reliability, Faculty of Materials and Manufacturing, Beijing University of Technology, Beijing 100124, China

Beijing Key Laboratory of Advanced Manufacturing Technology, Beijing University of Technology, Beijing 10012

Yinghua Liu

Department of Engineering Mechanics, AML, Tsinghua University, Beijing 100084, China

Haofeng Chen

Department of Mechanical & Aerospace Engineering, University of Strathclyde, Glasgow G1 1XJ, UK

[1] Corresponding authors: ywdai@bjut.edu.cn;

Abstract

Interface creep cracking is very common to be seen in various kinds of welded components which are used widely in engineering practice. In the present paper, the interface creep crack tip field by considering material mismatch effect is studied. The interface creep crack is found to be close to the HRR field which can produce the faster creep crack growth rate. A material mismatch constraint parameter is proposed based on the validation of the local mismatch effect on the interface creep crack tip field which also maintains the self-similarity. An averaged material mismatch constraint M^{*}_{avg} is presented to represent the material mismatch constraint effect. It reveals that the material mismatch constraint effect for interface creep decreases with the increase of the local mismatch factor. The physical meaning of the material mismatch constraint effect for the interface creep crack and its future application to engineering failure analysis is also discussed and presented.

Keywords: interface creep crack; stress field; material mismatch; self-similarity; material constraint;

Nomenclature

A_{B}	creep coefficient of base metal
A_{W}	creep coefficient of weld metal
a	crack length
α	coefficient of Ramberg-Osgood model
$C(t)$	$C(t)$-integral
C^*	C^*-integral
E	Young's modulus
ε_{ij}	strain tensor
ε_0	reference strain
$\dot{\varepsilon}_0$	reference strain with rate form
$\dot{\varepsilon}_{ij}$	creep strain tensor with rate form
ε^p	plastic strain
$\hat{h}_{ij}$	bound function of elastoplastic interface crack
$\tilde{h}_{ij}$	bound function of creep interface crack
J	J-integral
$\mathbf{K}$	complex stress intensity factor of elastic interface crack
K_{I}	mode I stress intensity factor
K_{II}	mode II stress intensity factor
$\tilde{p}_{ij}$	angular distribution function of material mismatch stress field
Q	Q-stress (geometry and loading constraint parameter)
m	mismatch factor $\left(A_{\mathrm{B}}/A_{\mathrm{W}}\right)^{1/n}$
m_{g}	mismatch factor $\left(A_{\mathrm{B}}/A_{\mathrm{HAZ}}\right)^{1/n}$
M^*	material constraint parameter

η	oscillatory parameter of elastic interface crack
v	Poisson's ratio
n	creep exponent
P	applied remote load
P_0	reference load
r	radial distance to crack tip
S_{ij}	deviatoric stress
θ	angular angle
t	creep time
t_{T}	transition creep time
σ_0	reference stress
σ_{ij}	stress tensor
$\tilde{\sigma}_{ij}$	dimensionless stress components
$\tilde{\sigma}_{ij}^{\mathrm{I}}$	dimensionless stress distribution function in part I material
$\tilde{\sigma}_{ij}^{\mathrm{II}}$	dimensionless stress distribution function in part II material
σ_{ij}^{M}	mismatch stress field
$\sigma_{ij}^{\mathrm{Ref}}$	reference stress field
T	*T*-stress
T_i	traction force
u_i	displacement
$\dot{u}_i$	displacement with rate form
w	width of crack plate

Abbreviations

BM	base metal
CEEQ	equivalent creep strain
CPE8R	eight node isoparametric plane strain element with reduced integration
FE	finite element
HAZ	heat affected zone
HRR	Hutchinson-Rice-Rosengren
MBLM	modified boundary layer model
SECP	single edge cracked plate
SIF	stress intensity factor
WM	weld metal

1 Introduction

Interfacial cracking is very common to be found in various kinds of weldment and dissimilar joints. It can be found frequently from the observation of experimental works that there are many interfacial creep cracks which lie in the fusion line of welding joints and welded components [1-6]. Characterization of interface crack plays a crucial role in the failure assessment of those welded structures and components. The accurate prediction of interfacial creep crack tip field is a preliminary to build up a reasonable assessment method for evaluating the interface creep crack growth. Tremendous attentions have been attracted to study the fracture of welding components from different viewpoints [7-12], among which characterization of interfacial creep crack tip field is one of the critical issues in those important topics. A full review on the fracture mechanics in weldment was given by Zerbst et al. [13].

Note that it is prerequiste to predict the failure behavior of those components, some works have been presneted to the study of the stresss field and fracture parameters for bimaterial interfacial creep crack. As for creeping solids, Tu [14] presented the tendency of $C(t)$-integral for crack tip field near the interface of a bimaterial. Yoon and Kim [15] presented the characterization of bimaterial creep crack with a sharp crack tip, and solutions of $C(t)$-integral were also provided. The advantage of using the sharp crack tip is that the numerical solution to $C(t)$-integral can be obtained easily by finite element (FE) codes, however, this does not coincide with the actual observation from experimental test of crack tip blunting effect at elevated temperature [16]. Kitamura et al. [17] presented the stress field for edge creep crack of a bimaterial and found that the stress highly concentrates near the interface edge. Ngampungpis et al. [18, 19] gave the singular stress field of bimaterial edge creep crack under a sustained load, and revealed the stress field near the interface edge with no or weak elastic stress singularity. A higher-order term theoretical analysis was carried out by Yuan and Yang [20] for an interfacial crack which locates between elastic base material and creeping material. The numerical investigations for stress field for a stationary interface creep crack under

plane strain condition and pure opening dominated mode were presented by Biner [21, 22], and the focus of the studies was the influence of layer width on stress field and C^*-integral amplitude.

Recently, the constraint effect for cracked weldment has attracted the great attention due to the importance of this topic and its potential implications in the industrial applications of welding components. Yang et al. [23, 24] presented the out-of-plane constraint effect for cracked weldment with experimental work, and a unified parameter was presented to characterize the constraint effect of dissimilar joints. Yamamoto et al. [25] also presented the experimental investigation on the constraint effect of a creep crack in welded joints. Dai et al. [26] reported the C^*-M^* two parameters approach to characterize the mismatch constraint effect of a creep crack located in the heat affected zone (HAZ) within the mismatched modified boundary layer (MBL) model. However, the investigations mentioned above are all based on the simplification that the crack locations are in the HAZ, while the significance in the characterization of constraint effect for bimaterial interface creep crack is definitely un-negligible.

As the singularity of interfacial creep crack may not satisfy the HRR [27, 28] type, the constraint parameters [29-34] which were proposed for homogeneous materials should be reconsidered for bimaterial interface creep crack. There are two difficulties for the characterizations of interfacial creep crack: (1) the singularity determination and the oscillation of crack tip field, e.g. the stresses of the interface crack tip field for linear elastic homogeneous material oscillate faster if the crack tip is approached as the influence of oscillatory singularity; (2) the fracture parameter characterization in bimaterial, e.g. complex stress intensity factor (SIF). Hence, the constraint effect characterization for interfacial creep crack is much more difficult compared with that in a homogeneous solid. As the existed difficulties mentioned above, only a few theoretical results have been made for bimaterial interface creep crack, e.g. the asymptotic analyses proposed for interface crack of mode II [35] and mode III [36] in bimaterial power law creeping solids show the singularity discrepancy from the HRR type. However, the investigations on the characterization of constraint effect for

interface creep crack almost have not been found in the available literatures to the authors' best knowledge. Moreover, the influence of material mismatch on interface creep crack tip field and the characterization of constraint effect caused by material mismatch have not been investigated yet though the influence of material mismatch on constraint effect in elastoplastic material has been investigated by some researchers [37-39].

According to the analogy between power law creep and power law elastoplasticity [40], the solution of the elastoplastic bimaterial problem can be a reference to the study of the bimaterial problem with power law creep. There were some studies on bimaterial interfacial crack of elastoplastic material under both small scale yielding and large scale yielding, as discussed by Shih and coworkers [41-43]. Wang [44] presented the asymptotic field analysis for bimaterial interfacial crack in a hardening elastoplastic material. For small scale yielding, the MBL model is generally used to analyze the constraint effect of crack. Zhang et al. [45] studied the constraint effect for bimaterial and tri-material, and also material constraint effect for mismatched weld metal with *J*-*M* approach. The *M*-parameter defined in [39, 45] characterizes the constraint effect caused by material mismatch for elastoplastic material and it is also a magnitude to represent the difference field caused by strength mismatch. Furthermore, the *M*-parameter is rather different with other parameters, e.g. the *Q*-parameter presented by O'Dowd and Shih [46] and A_2-parameter [47], which can characterize the constraint effect influenced by specimen geometry and loading level. Østby et al. [48] studied the constraint effect caused by residual stress and plastic work hardening with the MBL model. Lee and Kim [49] presented the constraint effect of interfacial crack for power law strain hardening bimaterial with the MBL formulation. Lately, extending the MBL model to evaluate the constraint effect of crack in creep regime has drawn the attention of some researchers. With the MBL model, the in-plane and out-of-plane constraint effects for creep crack in homogeneous materials were studied by Shlyannikov and coworkers [50, 51]. The mismatched MBL model with the HAZ was established to investigate the material constraint effect of creep crack by Dai et al. [33]. A more recent

work on discussing material constraint effect of center cracked weldment is also reported by our group [52].

The aim of this study is to make a thorough investigation on the characterization of mismatch constraint effect for interfacial creep crack. The stress fields of interfacial creep crack within the mismatched MBL model are analyzed and discussed. The two parameters approach of C^*-M^* [33] is developed to study the material constraint effect for interfacial creep crack. The M^*-parameter [33] is also developed to characterize the constraint effect of material mismatch for interfacial creep crack and it represents the magnitude of the difference field induced by the material mismatch. The overall structure of this paper is as follows. The theoretical background of the interfacial fracture mechanics and the concept of the material mismatch constraint effect are given in Section 2. Numerical procedures are illustrated in Section 3, and the results and discussions are presented in Section 4. Finally, the conclusions are given as a summary in Section 5.

2 Theoretical framework

For the case of a crack along the interface between two bonded linear elastic, isotropic and homogeneous materials, the crack tip stress field is presented as [53]

$$\sigma_{ij}(\theta,r)=\frac{1}{\sqrt{2\pi r}}\left\{\mathrm{Re}\left(\mathbf{K}r^{i\eta}\right)\tilde{\sigma}_{ij}^{I}(\theta,\eta)+\mathrm{Im}\left(\mathbf{K}r^{i\eta}\right)\tilde{\sigma}_{ij}^{II}(\theta,\eta)\right\} \tag{1}$$

where the complex SIF $\mathbf{K}=K_{\mathrm{I}}+iK_{\mathrm{II}}$, $i=\sqrt{-1}$, $\tilde{\sigma}_{ij}^{\mathrm{I}}(\theta,\eta)$ and $\tilde{\sigma}_{ij}^{\mathrm{II}}(\theta,\eta)$ are dimensionless angular functions. K_{I} and K_{II} are mode I SIF and mode II SIF, respectively. The constant η is the oscillatory parameter which can be given as follows:

$$\eta=\frac{1}{2\pi}\ln\left(\frac{k_1\mu_2+\mu_1}{k_2\mu_1+\mu_2}\right) \tag{2}$$

with

$$k_l = \begin{cases} 3-4\nu_l & \text{under plane strain} \\ (3-\nu_l)/(1+\nu_l) & \text{under plane stress} \end{cases} \tag{3}$$

where ν_l and μ_l $(l=1,2)$ are the Poisson's ratio and shear moduli for material 1 and material 2 which are shown in Fig. 1. The coordinate system used for bimaterial crack tip field is plotted in Fig. 1. Herein, the material 1 and material 2 in Fig. 1 are considered to be base metal and weld metal, respectively.

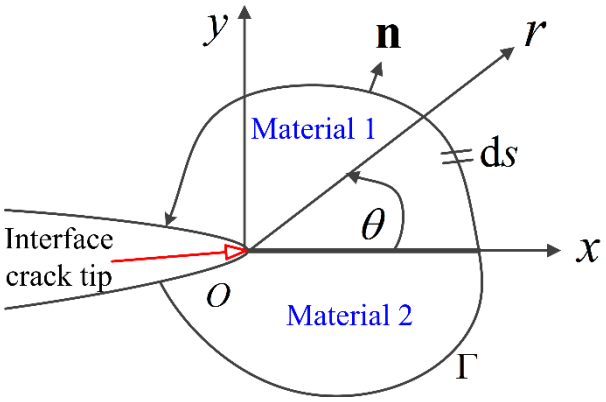

Fig. 1 Coordinate system for interface crack tip

From Eq. (1), the SIF of interfacial crack is a function of K_{I} and K_{II} if $\eta \neq 0$. To simplify the problem, the linear elastic properties of two materials are adopted to be the same during the analysis in this paper, i.e. $\eta = 0$. When η equals to 0, the interface crack will become standard mode I type or standard mode II type crack. In general, the elastic properties of two materials are simplified to be the same in engineering practices. Hence, the assumption with $\eta = 0$ is reasonable here.

The stress field for elastoplastic interfacial crack in Ramberg-Osgood materials under uniaxial state, which is defined as $\varepsilon^p/\varepsilon_0 = \alpha(\sigma/\varepsilon_0)^n$, presented by Shih and Asaro [41, 42] can be written as:

$$\sigma_{ij}(\theta, r) = \sigma_0 \left(\frac{J}{\alpha \sigma_0 \varepsilon_0 r} \right)^{1/(n+1)} \hat{h}_{ij}\left(\theta, r/(J/\sigma_0), \xi\right) \tag{4}$$

where σ_0, ε_0 and α are the reference stress, the reference strain and the coefficient of Ramberg-Osgood model, respectively. In Refs. [41-43], σ_0, ε_0 n, and α adopt the constants of weaker part material. ξ is the phase parameter. $\hat{h}_{ij}$ is a bound

function which is slowly changed with $r/\left(J/\sigma_0\right)$.

It can be found that Eq. (4) is the HRR-like. Based on the analogy between power-law creep and power-law plasticity, the stress field for the interfacial creep crack also should be the HRR-like type according to Biner [21, 22], and the standard HRR type solution for creep crack is written as following.

$$\sigma_{ij}\left(\theta,r\right)=\sigma_0\left(\frac{C\left(t\right)}{\sigma_0\dot{\varepsilon}_0 I_n r}\right)^{1/(n+1)}\tilde{\sigma}_{ij}\left(\theta,n\right) \tag{5}$$

in which $C\left(t\right)$ and $\dot{\varepsilon}_0$ are $C\left(t\right)$-integral and the reference strain rate, respectively.

According to the aforementioned numerical solutions under both transient and extensive creep range [21, 22], the interface creep crack tip field resembles the HRR solution closely for the material part under larger creep coefficient. Here, we present that the stress field of an interface creep crack by taking the geometry constraint into account as the following form.

$$\frac{\sigma_{ij}}{\sigma_0}=\left(\frac{C^*}{\sigma_0\dot{\varepsilon}_0 r}\right)^{1/(n+1)}\tilde{h}_{ij}\left(\theta,n\right)+Q\left(\theta,n\right)\delta_{ij} \tag{6}$$

For those resembled HRR type interface crack, the Q stress in Eq. (6) can be defined as the hydrostatic stress given by O'dowd and Shih [46] in elastoplastic material as well as the creep crack [32]. The Q stress also can be treated as the difference of opening stress between the solutions of full field and referenced field as discussed by Budden and Ainsworth [29].

Based on our reported work [33], the stress field for an interface creep crack should be characterized as below if multilayered materials are taken into consideration.

$$\frac{\sigma_{ij}^{M}}{\sigma_0}=\left(\frac{C^*}{\sigma_0\dot{\varepsilon}_0 r}\right)^{1/(n+1)}\tilde{h}_{ij}\left(\theta,n\right)+Q\left(\theta,n\right)\delta_{ij}+M^*\left(\theta,n\right)\tilde{p}_{ij} \tag{7}$$

in which the third term is only caused by material mismatch, M^* is the material mismatch constraint parameter and $\tilde{p}_{ij}$ is the angular distribution function which is similar to those definition of $\tilde{h}_{ij}$. If a reference field is selected, the mismatched stress field for an interface creep crack tip field can be presented as

$$\sigma_{ij}^{\mathrm{M}} = \sigma_{ij}^{\mathrm{Ref}} + M^{*}\sigma_{0}\tilde{p}_{ij}\left(\theta, n\right) \tag{8}$$

The selection of reference stress field $\sigma_{ij}^{\mathrm{Ref}}$ should be a stress field which should not take the material constraint into account. For the interface creep crack, the reference field should choose the interface creep crack which is resembled the HRR filed without the material mismatch. For Eq. (7) and Eq. (8), the method can be degenerated to the problem with a crack located in a HAZ which was presented by Dai et al. [33].

3 Numerical procedures

In order to analysis a series solutions and characterizations for interface creep crack tip field, two plane strain models with interface creep crack, i.e. modified boundary layer model (MBLM) and single edge cracked plate (SECP), are adopted to perform the numerical simulations (see Fig. 2).

For the mismatched MBLM, a circular plate with two materials is considered, i.e. base metal in the upper part of plate and weld metal in the lower part of plate. The approximation of near crack tip field is obtained with the application of boundary conditions imposed by analytical displacements of mode I crack in linear elastic material. For two dimensional plane strain problem, the displacement conditions for far field K_{I} considering the T-stress can be expressed as

$$\begin{cases} u_{x} = \dfrac{K_{\mathrm{I}}}{E}\sqrt{\dfrac{r}{2\pi}}\left(1+\nu\right)\left(3-4\nu-\cos\theta\right)\cos\dfrac{\theta}{2} + \dfrac{T}{E}\left(1-\nu^{2}\right)r\cos\theta \\ u_{y} = \dfrac{K_{\mathrm{I}}}{E}\sqrt{\dfrac{r}{2\pi}}\left(1+\nu\right)\left(3-4\nu-\cos\theta\right)\sin\dfrac{\theta}{2} - \dfrac{T}{E}\nu\left(1+\nu\right)r\sin\theta \end{cases} \tag{9}$$

where E is the Young's modulus, K_{I} represents the stress intensity factor (SIF), T is the T-stress term, ν is the Poisson ratio and θ is the polar angle shown in Fig. 2. The radius of the MBLM is 1000 mm so that the small scale creep can be approached if there is only the applied K-field at the outer boundary. For SECP specimen with interface creep crack, the height and width are kept as 125 mm and 50 mm, respectively. The extensive creep will be obtained easily if the applied remote loading is large enough

with a sustained creep time.

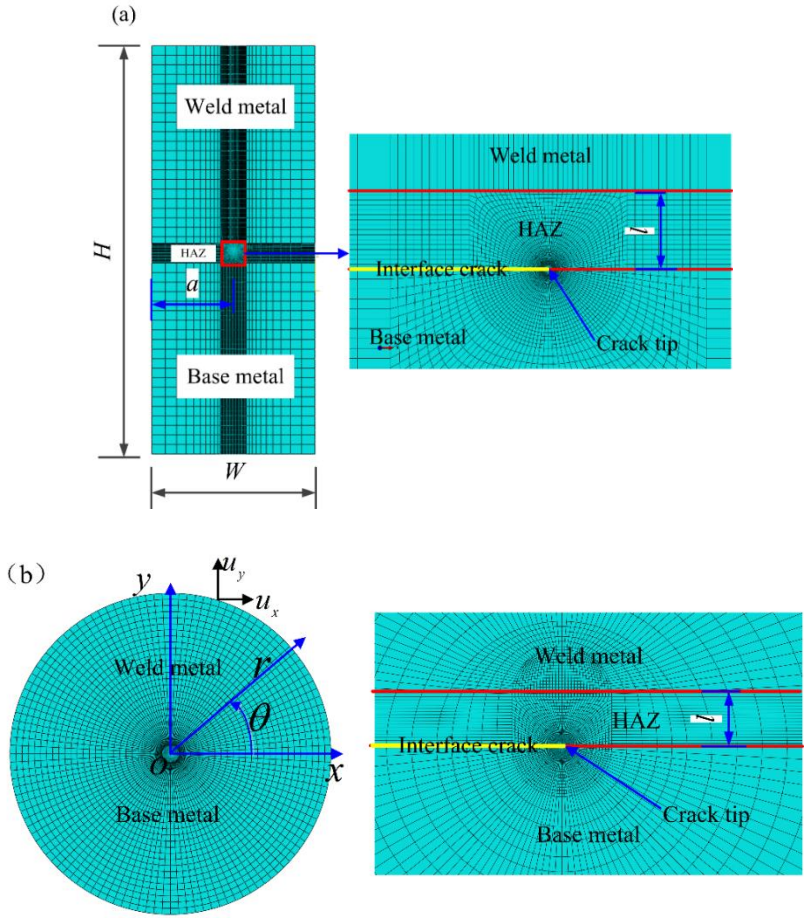

Fig. 2 The configurations and FE meshes of (a) SECP and (b) MBLM as well as crack tips

In order to carry out the numerical analyses, the FE code ABAQUS [54] is used. In this article, the focus of problem is a two-dimensional plane strain problem. The global FE model is shown in Fig. 2, and the element type is selected as CPE8R, i.e. the eight node plane strain element using reduced integration. The loading conditions are shown in Fig. 2 , where the displacement boundaries are controlled by the K_{I}-field in Eq. (9) for MBLM. The element numbers for MBLM and SECP are 12120 and 8148 with a refined crack tip. The FE meshes of these analyzed models are kept the same for all the computations of the present study. For the convenience of data extracting, the crack tip is defined as the coordinate origin. It should be noted that the FE code can extract the $C(t)$-integral accurately and robustly for the interface creep crack. The FE solutions are accurate enough to extract the stress and strain field of interface creep crack. Thus, other methods such as finite element over deterministic method [55, 56]

to determine the stress and strain of interface crack is not used in the current work, and it will be discussed in future work.

The power-law type, so called Norton's constitutive equation, is adopted in this study and the form of it is presented as

$$\dot{\varepsilon} = \frac{\dot{\sigma}}{E} + \dot{\varepsilon}_0 \left(\frac{\sigma}{\sigma_0} \right)^n \tag{10}$$

in which E, n, $\dot{\sigma}$, $\dot{\varepsilon}_0$ and σ_0 are the Young's modulus, creep exponent, stress rate, reference creep strain rate and reference stress, respectively. As usual, the creep coefficient is presented as $A = \dot{\varepsilon}_0 / \sigma_0^n$. Herein, A_B and A_W denote the creep coefficients of the base metal and weld metal, respectively. The creep mismatch factor m and m_g are defined as:

$$m = \left(\frac{A_B}{A_W} \right)^{1/n} \tag{11}$$

$$m_g = \left(\frac{A_B}{A_{HAZ}} \right)^{1/n} \tag{12}$$

Table 1 Material constants used in calculations with the same creep exponent

A_B	A_W	A_{HAZ}	m	m_g	n
3.20E-11	1.60E-10	1.92E-10	0.58	0.55	3
3.20E-11	8.00E-11	3.84E-11	0.74	0.94	3
3.20E-11	3.20E-11	3.20E-11	1.00	1.00	3
3.20E-11	8.00E-12	7.96E-12	1.59	1.59	3
3.20E-11	4.00E-12	5.31E-12	2.00	1.82	3
3.20E-11	1.60E-10	1.92E-10	0.58	0.55	3
3.20E-11	1.60E-10	3.84E-11	0.58	0.94	3
3.20E-11	1.60E-10	3.20E-11	0.58	1.00	3
3.20E-11	1.60E-10	7.96E-12	0.58	1.59	3
3.20E-11	1.60E-10	5.31E-12	0.58	1.82	3
3.20E-11	4.00E-12	1.92E-10	2.00	0.55	3
3.20E-11	4.00E-12	3.84E-11	2.00	0.94	3
3.20E-11	4.00E-12	3.20E-11	2.00	1.00	3
3.20E-11	4.00E-12	7.96E-12	2.00	1.59	3
3.20E-11	4.00E-12	5.31E-12	2.00	1.82	3

During the calculations, elastic properties of base metal and weld metal are treated

to be the same to simplify the problem, i.e. Young's modulus and the Poisson's ratio of two materials are adopted as 160 GPa and 0.3, respectively. The creep coefficients adopted in this paper are given in Table 1 where the material properties come from [57]. The undermatch condition is considered to be m<1 (or m_g <1) and the overmatch condition is defined as m > 1 (or m_g >1).

The $C(t)$-integral here is same as that defined by Bassani and McClintock [58] with the domain integral method presented by Li et al. [59], which can be extracted from the finite element results directly. For the interface creep crack, the $C(t)$-integral is still valid, which has been validated by Yoon and Kim [15], and presented as below [58, 59]:

$$C(t)=\int_{\Gamma\to 0} W^{*}\mathrm{d}y-T_i\left(\frac{\partial \dot{u}_i}{\partial x}\right)\mathrm{d}s \tag{13}$$

where, as shown in Fig. 1, Γ is a counterclockwise integration contour around the crack tip, and T_i, $\dot{u}_i$, $\mathrm{d}y$ and $\mathrm{d}s$ are the traction vector on Γ, the displacement rate, the increments in y-direction and along Γ, respectively. To improve the accuracy, fifteen contours are averaged to be the $C(t)$-integral under transient creep and the C^{*}-integral under the extensive creep in all these calculations.

4 Results and discussions

4.1 C^{*}-integral and creep zone

To characterize the interface creep crack, the $C(t)$-integral should be discussed firstly as it will determine the amplititude of the first order term for interface creep crack. In Fig. 3, variations of $C(t)$ with creep time for the MBLM (Fig. 3(a)) and the SECP (Fig. 3(b)) are presented. As the extensive creep is hardly approached for MBLM, the creep time without normalization is directly used, however, the transition creep time, t_{T}, defined in Eq. (14), is used to normalize the creep time for SECP as the extensive creep can be obtained quite conveniently.

$$t_T = \frac{(1-v^2)K^2}{(n+1)EC^*} \tag{14}$$

in which C^*, K, E, n, and v are the C^*-integral, stress intensity factor (SIF), Young's modulus, creep exponent and Poisson's ratio, respectively.

For the homogeneous creep crack tip field, there are some expressions to evaluate C(t) and C* integral for creep crack based on the analogy between the power-law creep and power-law plasticity. $C(t)$ under transient creep should be evaluated as below according to the analysis of HRR singularity for the power-law creep crack tip field by [60].

$$C(t) = \frac{(1-v^2)K^2}{(n+1)Et} \tag{15}$$

For the SECP, the C^*-integral with a homogeneous crack can be elevated as follow [61]:

$$C^* = B(w-a)(a/w)h_1(a/w,n)(P\sigma_0/P_0)^{n+1} \tag{16}$$

where P, P_0 and $h_1(a/w,n)$ are the applied remote loading, the reference load and the dimensionless geometry function. The reference load for homogeneous material is given as below [61]

$$P_0 = 1.45\chi(w-a)\sigma_{ys} \tag{17}$$

in which

$$\chi = \left(1+\left(\frac{a}{w-a}\right)^2\right)^{0.5} - \left(\frac{a}{w-a}\right) \tag{18}$$

The reference load of a bimaterial SECP is presented as follow if the yielding stress, σ_{ys}, of the base metal and weld metal are considered to be the same [61]:

$$P_0 = \frac{4}{\sqrt{3}}(w-a)\sigma_{ys} \tag{19}$$

In order to validate the applicability of the aforementioned formulae to evaluate the C^*-integral for the interface creep crack, the comparison between the finite element (FE) results and the estimations of these analyzed equations are given in as the following.

The $C(t)$-integral or C^*-integral values for MBLM model and SECP specimens are presented in Fig. 3. Clearly, it can be seen that the $C(t)$-integrals under MBLM are very

close to each other as if the creep time is greater than 10 hours. It should be noted that the estimation value computed by Eq. (14) is originally based on HRR assumption, i.e. the crack tip stress field obeys HRR singularity. However, the creep strain is much less than elastic strain during the beginning of the creep simulation which leads to that the crack tip deviates from the HRR assumption significantly, and this finally leads to the discrepancy between the estimation and numerical computations. Meanwhile, the estimation of Eq. (15) agrees to the FE solutions quite well though the $C(t)$-integrals are obtained for bimaterials. The C^* of the SECP specimens with the bimaterial are presented in Fig. 3(b). The path-independent $C(t)$-integral of interface creep crack in bimaterial SECP specimens are 0.00287 Nmm/h, 0.001685 Nmm/h, 9.65E-4Nmm/h, 0.000601 Nmm/h, 0.000539 Nmm/h, respectively. It implies that the C^*-integral decreases with the increase of general mismatch factor. As the applied loads in these cases are all the same, i.e. 10 MPa, the variation of the C^*-integral is considered to be influenced by the material mismatch only.

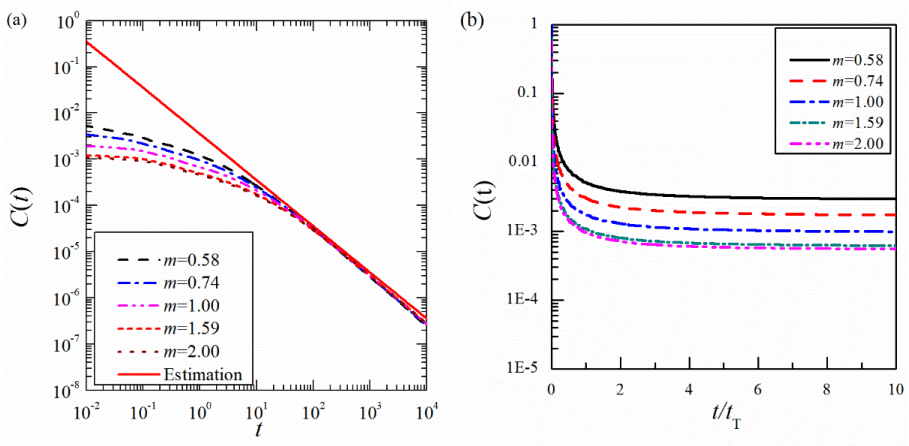

Fig. 3 Variation of $C(t)$-integral with creep time under different mismatch factors for (a) MBLM and (b) SECP

Though the $C(t)$-integral for the bimaterial interface creep crack has been presented in Fig. 3, the local material mismatch effect should be also considered as the there may exist the difference between the effect of local mismatch and general mismatch. As such, the local mismatch effect on the interface creep crack are given in Fig. 4. Two typical cases are selected here, i.e. $m=0.58$ and $m=2.00$. It can be found that the local material mismatch does influence the value of the C^*-integral as the values for

these cases are totally different. To state this point clearly, the C^*-integral under various mismatch factors are given in Table 2. It seems that the influence of the material mismatch on C^*-integral is very significant. In general, it can be found that the case with the lower general mismatch factor presents the higher C^*-integral. For overmatched general mismatch factor, the material mismatch effect on C^*-integral is less remarkable than that of undermatch condition.

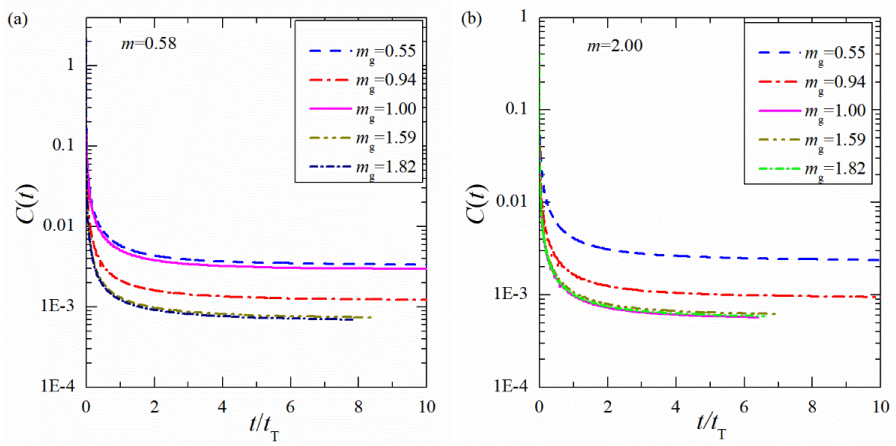

Fig. 4 Variation of $C(t)$-integral with normalized creep time: (a) m=0.58 and (b) m=2.00

Except for the $C(t)$-integral, the creep zone size is also an important factor which needs to be considered. Isoline of equivalent creep strain with level of 0.2% for interface creep crack with different mismatch factors at $t = 10t_T$ are presented in Fig. 5. Obviously, the creep zone shape for the interface creep crack varies with the change of mismatch factor. For the undermatched cases, i.e. m < 1.0, the creep boundary of the weld metal part is larger than that of the lower part, i.e. base metal. For the homogeneous case, the creep zone is symmetric about the crack line. For overmatch conditions, i.e. m >1.0, the lower part creep zone size is greater than that of upper part of the material.

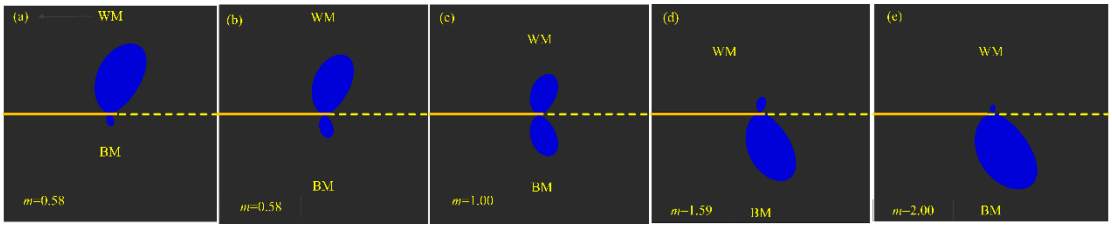

Fig. 5 Isoline of equivalent creep strain with level of 0.2% for interface creep crack with different mismatch factors at $t = 10t_T$

Isoline of equivalent creep strain with level of 0.2% for m=0.58 considering

mismatch effect at $t=10t_T$ is presented in Fig. 6. The local mismatch effect on the shape of the creep zone for interface creep crack is rather different. For lower mismatch factor, there exists the creep zone region for m_g<1.0 in both HAZ region and weld metal region, and the creep zone in base metal is less than that in weld metal. However, the creep strain only exists in HAZ and base metal region for m_g>1.0.

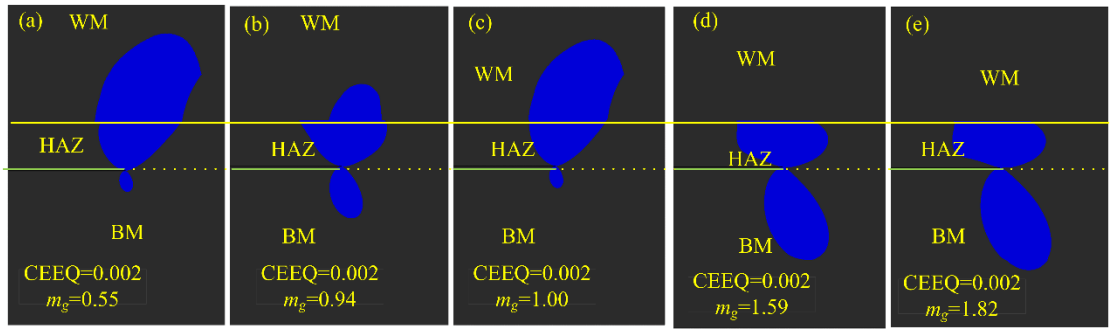

Fig. 6 Isoline of equivalent creep strain with level of 0.2% for m=0.58 considering mismatch effect at $t=10t_T$

For m=2.0, the variation tendencies are quite different from those of the undermatch case. The creep region for m_g<1.0 becomes discontinuous across the interface between HAZ and weld metal. However, the creep zone is very similar to that of m_g=1.0 for local overmatch mismatch case. These results imply the local material mismatch influence the interface creep crack totally different.

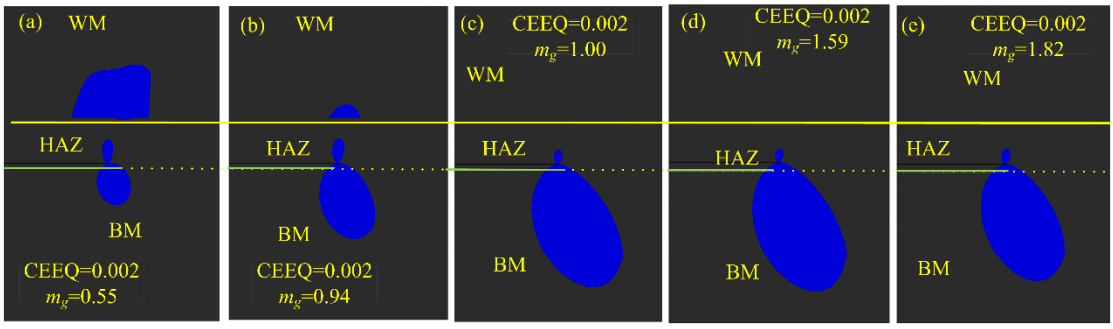

Fig. 7 Isoline of equivalent creep strain with level of 0.2% for m=2.00 considering mismatch effect at $t=10t_T$

4.2 Stress field of interface creep crack

As given in previous Section 4.1, the material mismatch not only causes the variation of C^*-integral, but also will lead to the change of C^*-integral. A mismatch constraint factor will be proposed based on the difference field analysis. To characterize

the radial stress components more clearly, a normalized distance presented below is adopted.

$$\bar{r} = \log\left(r\dot{\varepsilon}_0\sigma_0 / C(t)\right) \tag{20}$$

in which r is the true distance away from crack tip field.

4.2.1 Transient analysis

Fig. 8 presents the comparisons of angular stress distributions between HRR solutions and FE calculations. The HRR solutions given here are presented with two values in which one is calculated with the weld metal material constants, denoted with HRR WM, while another is analyzed with the pure base metal constants, denoted with HRR BM. The variations of $C(t)$-integrals for MBLM are figured out in Fig. 8(a). All the angular stress distributions given in Fig. 8 are obtained with a distance away from crack tip 0.1 mm at the creep time of 10000 hours. The results show that only the radial stress is discontinuous across the interface in these stress components. It can be found that the stress components calculated with FE agree quite well with the HRR solutions which are computed with a larger creep coefficient regardless of undermatch or overmatch. The larger creep coefficient means that the creep strain accumulation rate will be faster. For homogenous MBLM, the agreement between HRR field and FE solutions is quite perfect as the distance is not significant and the T-stress term doesn't exist. According to the earlier analysis by Biner [21, 22], the angular stress distributions of the interface crack in the faster creeping sector resembles the HRR stress singularity at steady state creep. However, the conclusion still exists for small scale creep within the MBLM according to our numerical solutions.

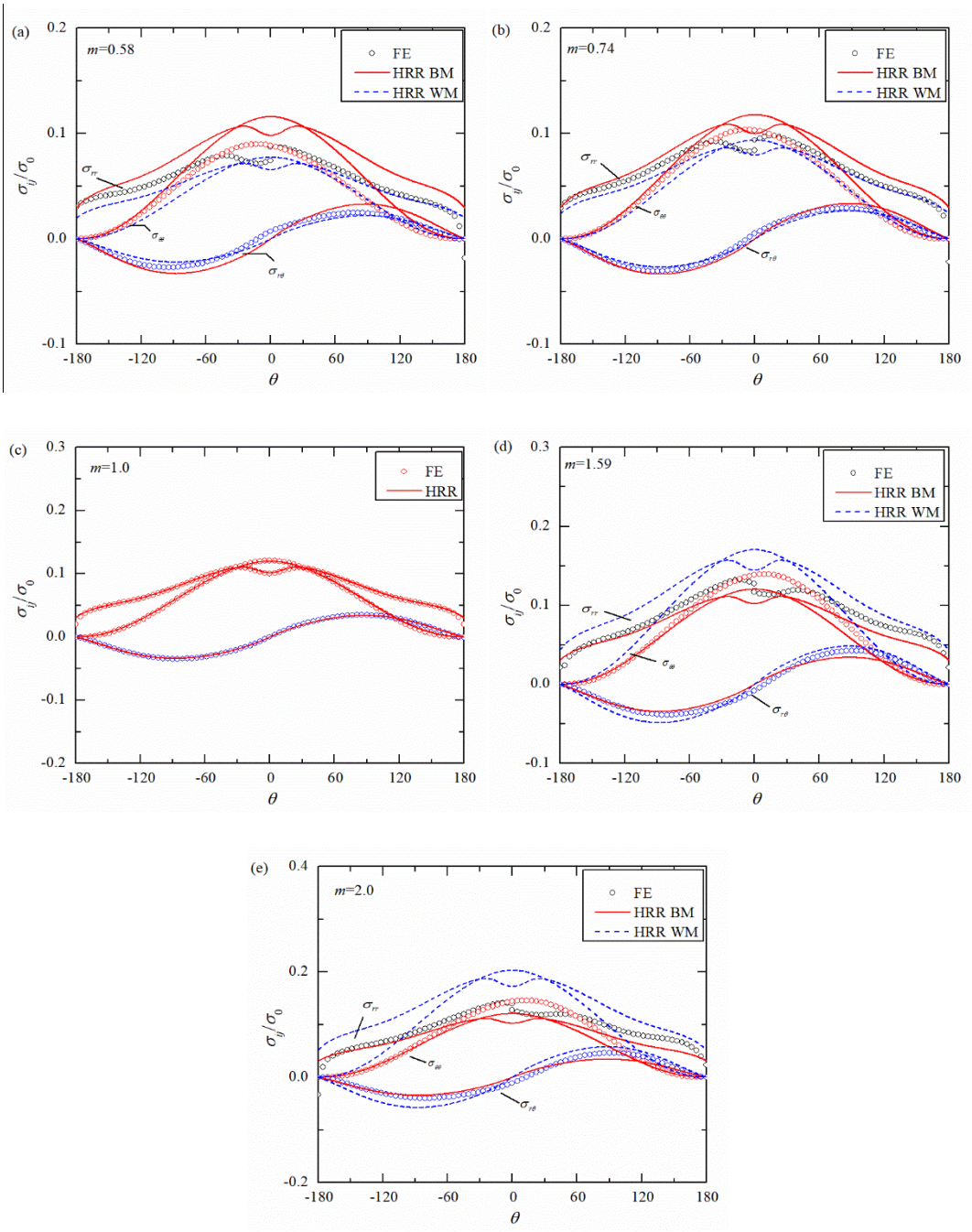

Fig. 8 Comparisons of angular stress distributions for MBLM with different mismatch factors

As discussed earlier of this section, the stress field for an interface crack can be written as:

$$\frac{\sigma_{ij}}{\sigma_0}=\left(\frac{C(t)}{\sigma_0\dot{\varepsilon}_0 r}\right)^{1/(n+1)}\tilde{h}_{ij}(\theta,n) \tag{21}$$

where $\tilde{h}_{ij}(\theta,\bar{r},n)$ is the angular distribution functions, σ_0 and $\dot{\varepsilon}_0$ are the selected reference stress and reference strain. By normalization of the Mises equivalent stress

with maximum value 1 with the similar method found in [62, 63], angular distribution functions of interface creep crack, $\tilde{h}_{ij}(\theta,n)$, in angular direction can be obtained and presented in Fig. 9. The radial stress components are jump across the interface and the others stress components are continuous at the interface. It can be seen that the angular distribution functions for m=1 agree quite well the HRR solutions which implies the rationality of the adopted method.

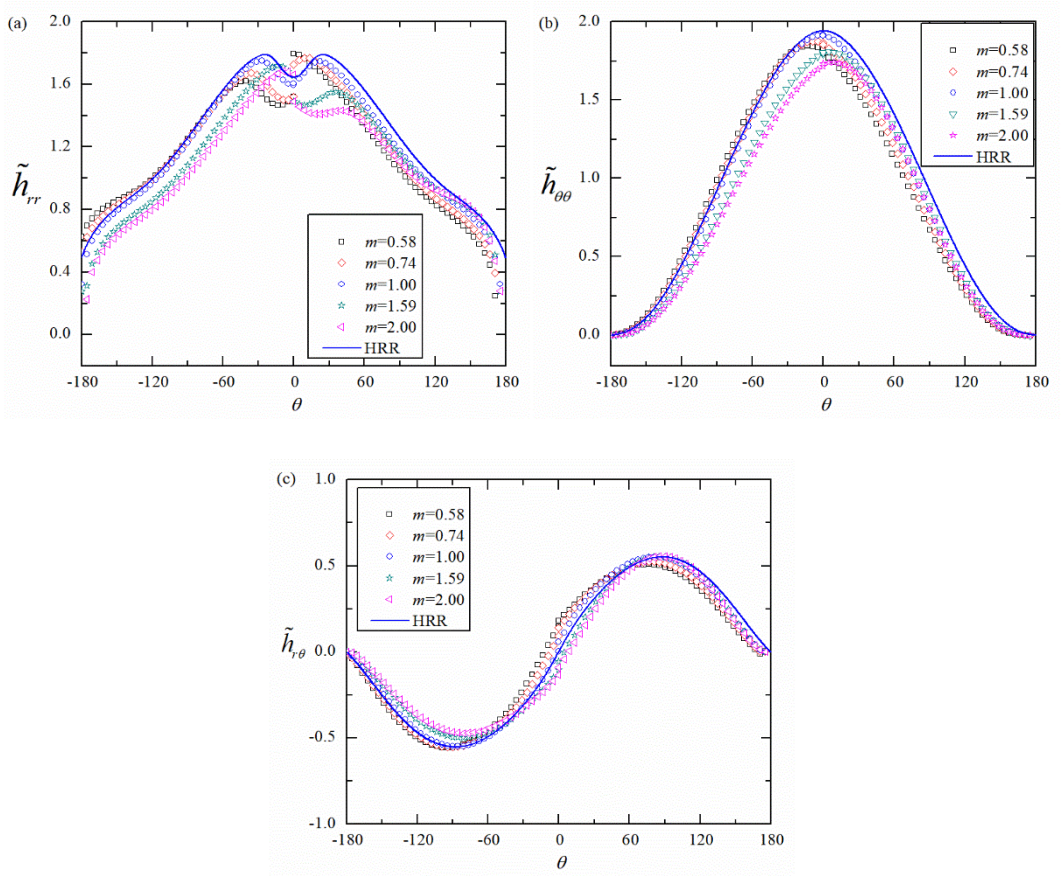

Fig. 9 Angular distributions of interface creep crack tip for (a) radial stress, (b) tangential stress and (c) shearing stress

4.2.2 Steady state analysis

For the steady state case, the stress field for interface creep crack is presented as below:

$$\frac{\sigma_{ij}}{\sigma_0}=\left(\frac{C^*}{\sigma_0\dot{\varepsilon}_0 r}\right)^{1/(n+1)}\tilde{h}_{ij}(\theta,n) \tag{22}$$

In order to describe the steady state interface creep crack tip field, the angular stress distributions functions and the comparisons between FE results and HRR solutions are presented in Fig. 10. These solutions are extracted from FE results for SECP at the creep time of $10t_T$ at r=1 mm. In these solutions, it can be found that dimensionless angular stress distributions calculated by FE coincides with the HRR WM solutions quite well if mismatch factor m is less than 1 or the larger creep coefficient case. Otherwise, the FE results agree quite well with the HRR BM solutions well if mismatch factor m is greater than 1, the larger creep coefficient case. For the homogeneous case (shown in Fig. 10(c)), the discrepancies between the HRR field and the FE solutions are considered to be the geometry constraint effect which is induced by specimen geometry or crack depth.

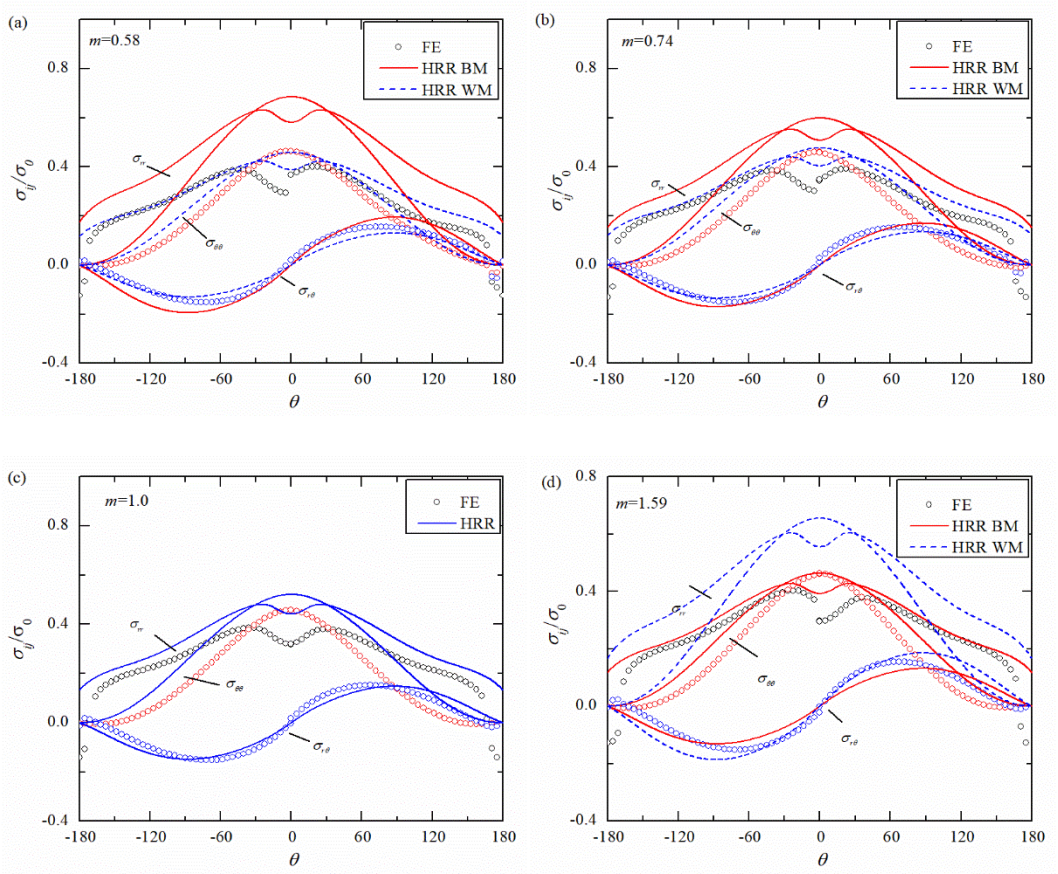

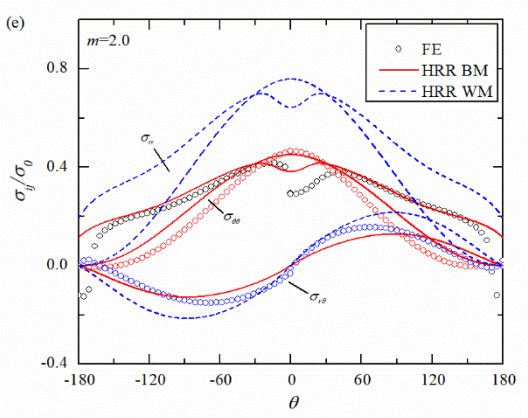

Fig. 10 Comparisons of angular stress distributions for SECP with different mismatch factors

To verify the self-similar properties of the interface creep crack, the radial and circumferential stress distributions along $\theta = 3^{\circ}$ and $\theta = -3^{\circ}$ are given in Fig. 11. It can be seen that the normalized radial stress and circumferential stress resemble the HRR solutions with m=1 very well, especially the values of opening stress. Hence, the self-similar property still exists for interface creep crack.

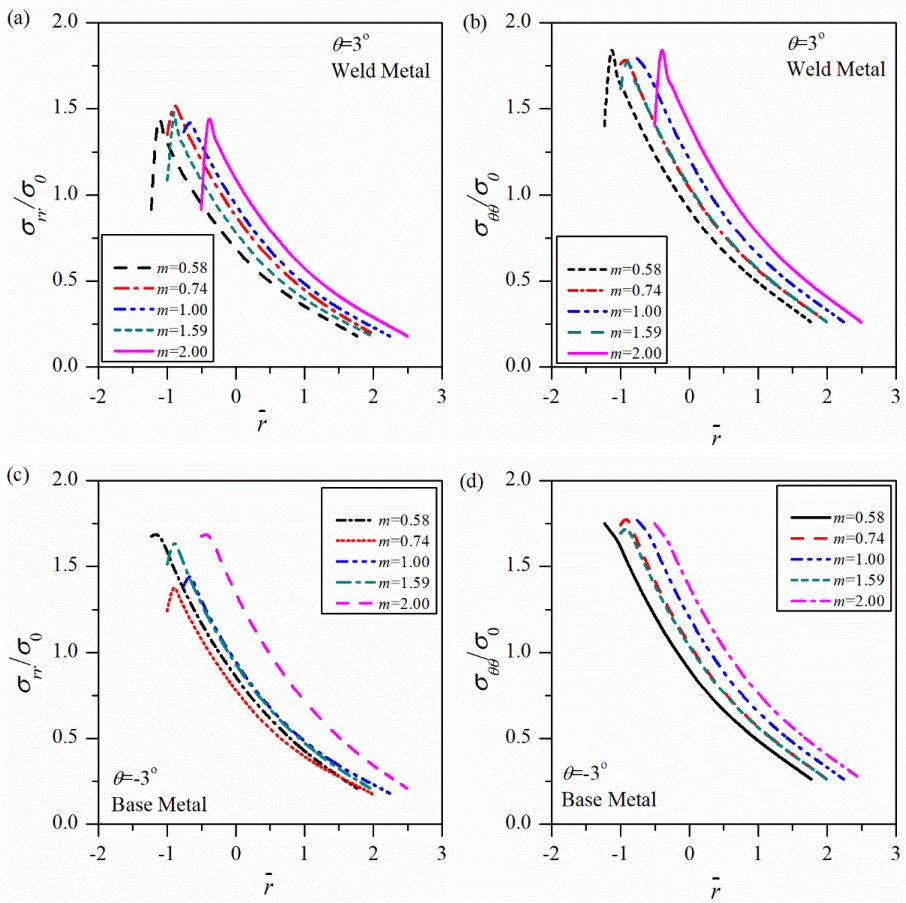

Fig. 11 Normalized radial stress distributions along $\theta = 3^{\circ}$: (a), (b) and $\theta = -3^{\circ}$: (c), (d)

4.3 Mismatch effect on interface creep crack in SECP

To quantify the mismatch effect on the interface creep crack in SECP specimen, the dimensionless angular stress distributions at $t=10t_{\mathrm{T}}$ are given in Fig. 12. The blue and red lines in Fig. 12 represent the HRR solutions obtained with the constant material properties of the pure base metal and the pure weld metal, respectively. From Fig. 12, it can be found that the dimensionless stress components with m_{g}=1.0 coincide with the HRR results calculated with weld metal quite closely. In general, the dimensionless angular stress distributions deviate from the HRR field quite large with the increase of the local mismatch factor. It reveals that the material mismatch that in the weld metal part can influence the interface creep crack tip field quite significantly.

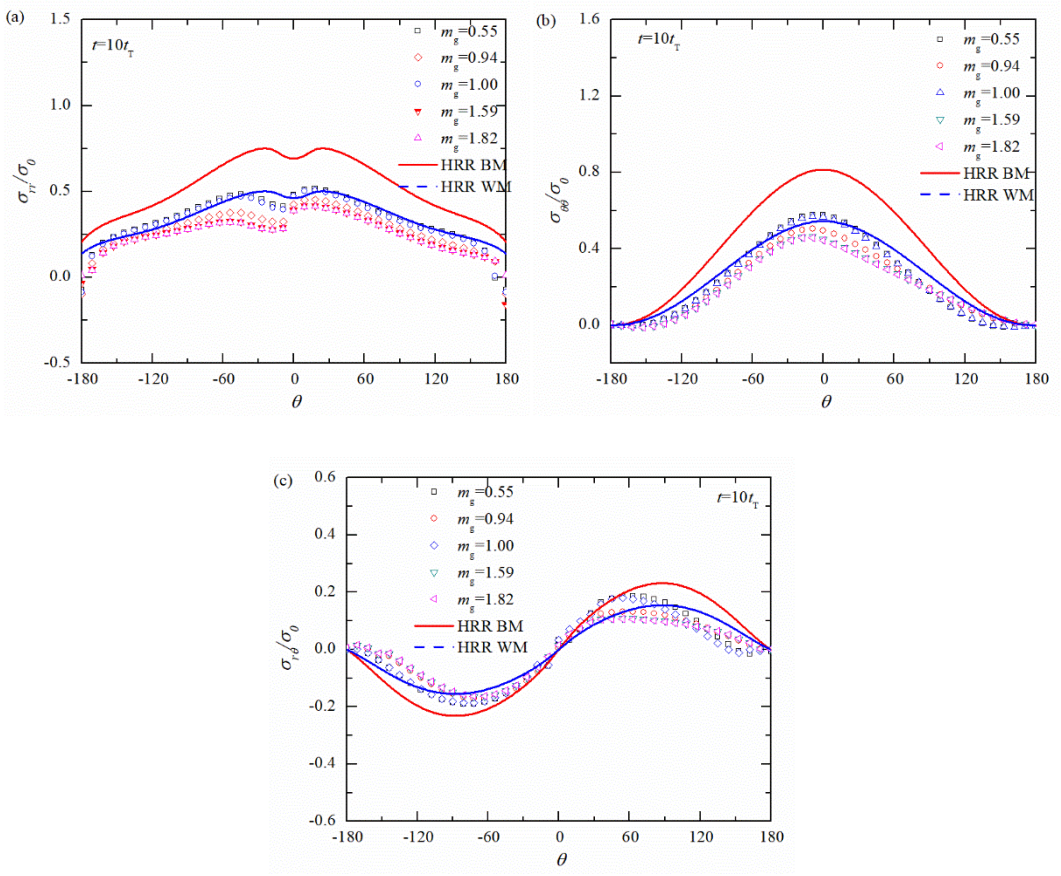

Fig. 12 Dimensionless angular stress distributions at $t=10t_{\mathrm{T}}$ under various mismatch factors for general mismatch factor m=0.58

To characterize the material mismatch effect, the dimensionless radial stress distributions at $\theta=-3^{\circ}$ are given in Fig. 13. It can be seen that the value of the

normalized distance $\bar{r}$ is between -2 and 2. The tendencies for radial stress components, angular stress components and shearing stress components under different local mismatch factors resemble with each other quite well. However, it should be mentioned that the amplitude for these stress components are totally different, which also implies the material mismatch effect. Compared with the HRR solutions of the base metal, the stress components are lower. For $\theta = 3^{\circ}$, the tendencies for these radial stress components shown in Fig. 14 are quite similar to those conditions of $\theta = -3^{\circ}$.

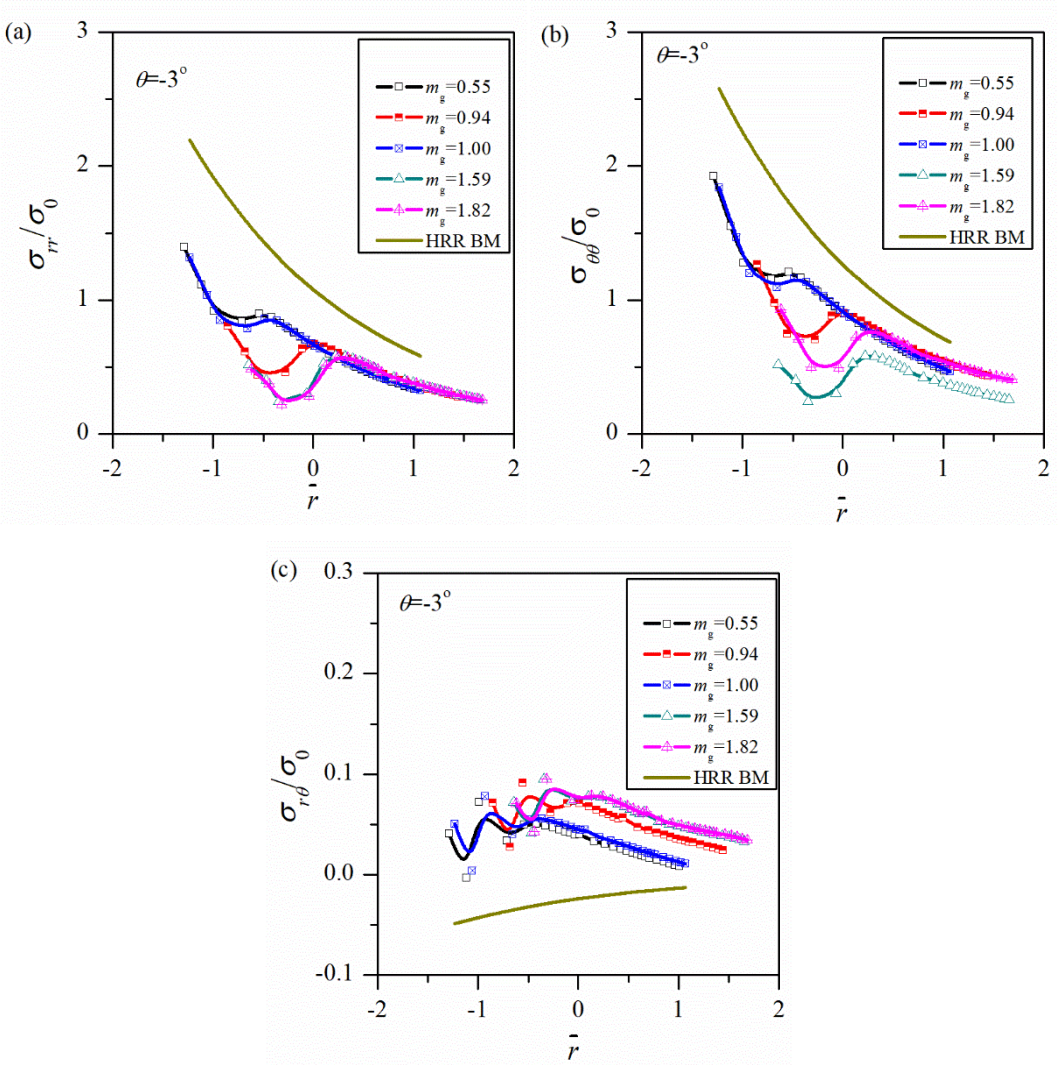

Fig. 13 Dimensionless stress distributions in radial direction along θ=-3° under various mismatch factors for m=0.58

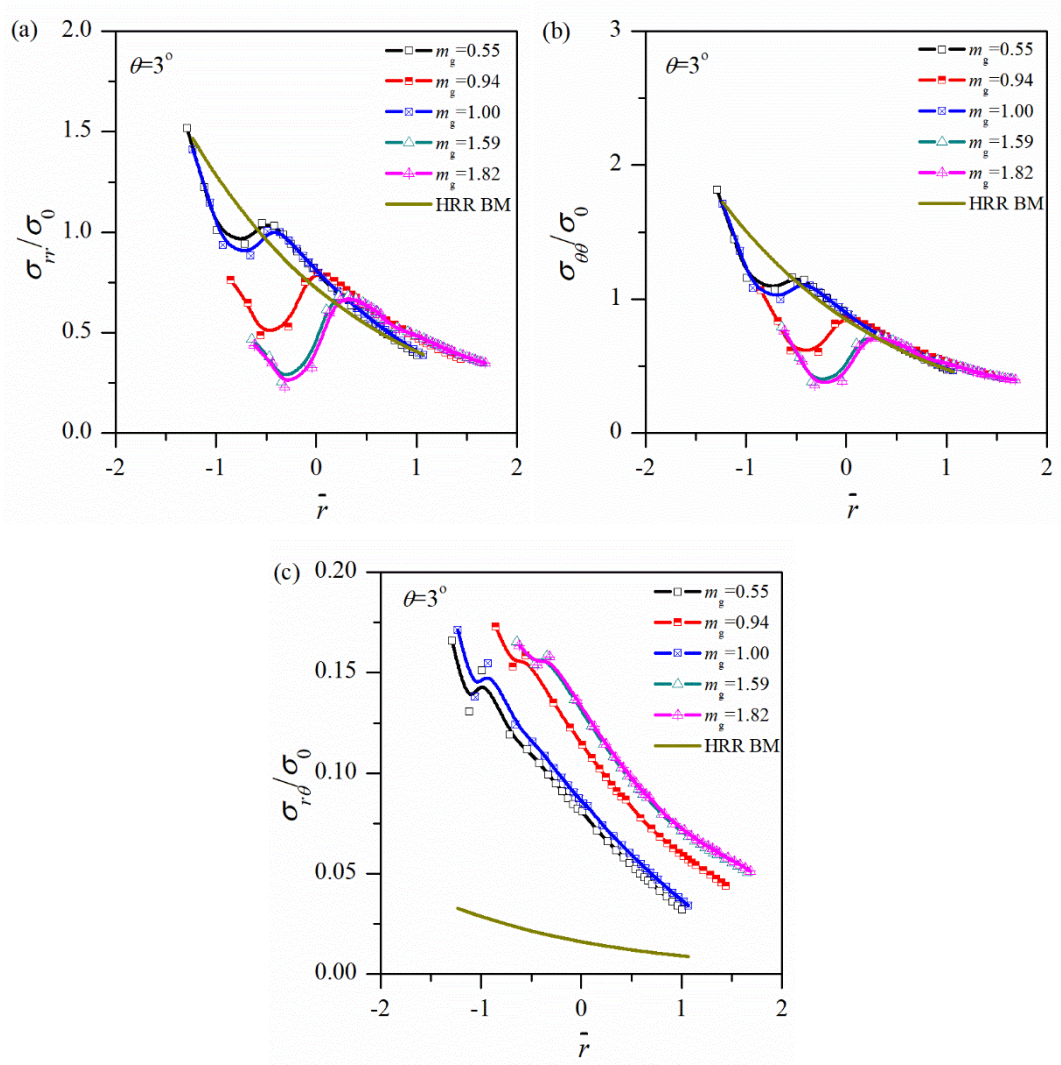

Fig. 14 Dimensionless stress distributions in radial direction along θ=3° at $t=10t_T$ under various mismatch factors for general mismatch factor m=0.58

Considering the general mismatch m=2.0, the dimensionless angular stress distributions are presented in Fig. 15. It can be found that the angular stress distributions with m_g =1.0 approaches to the HRR solutions not that closely as the creep zone under this condition is much smaller than that of the m=0.58. However, the stress components given here still can verify the effect of the material mismatch under local overmatch condition.

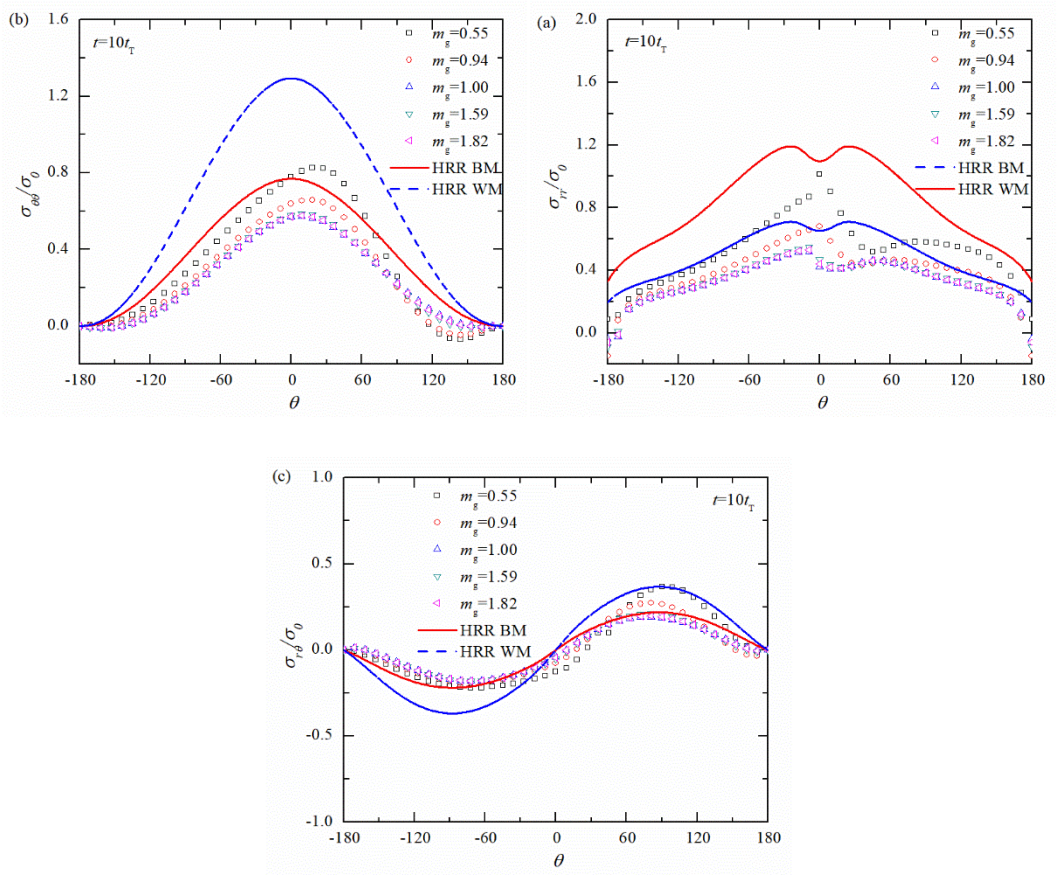

Fig. 15 Dimensionless angular stress distributions at $t=10t_T$ under various mismatch factors for m=2.00

The radial distributions for radial stress, angular stress and shearing stress along $\theta=3^o$ and $\theta=-3^o$ are presented in Fig. 16 and Fig. 17, respectively. It can be found that the dimensionless stress components under local overmatch conditions are still similar to each other very much in the region of normalized distance -2 and 2. Again, the stress components here are less than that of the HRR solutions calculated with weld metal.

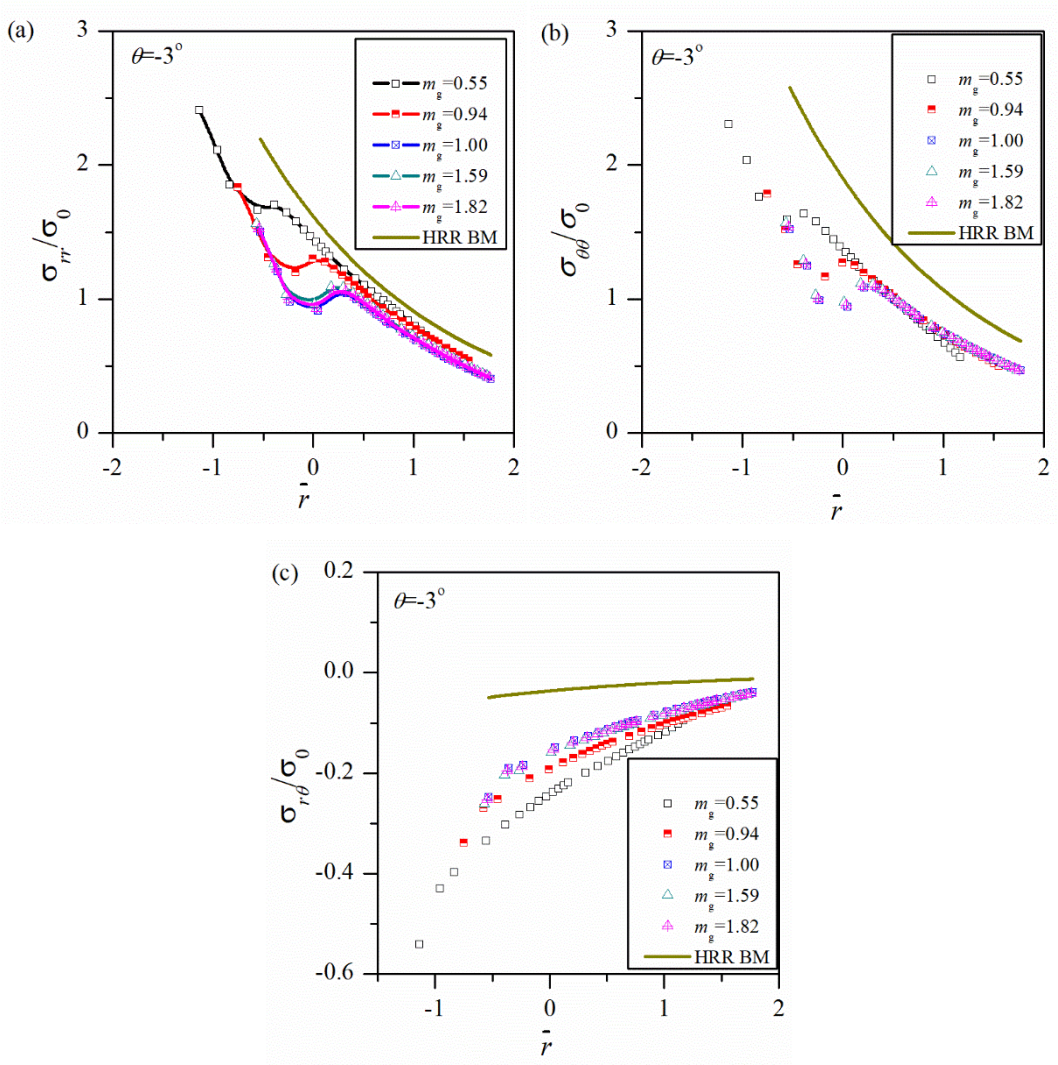

Fig. 16 Dimensionless stress distributions in radial direction along θ=-3° at $t=10t_T$ under various mismatch factors for m=2.00

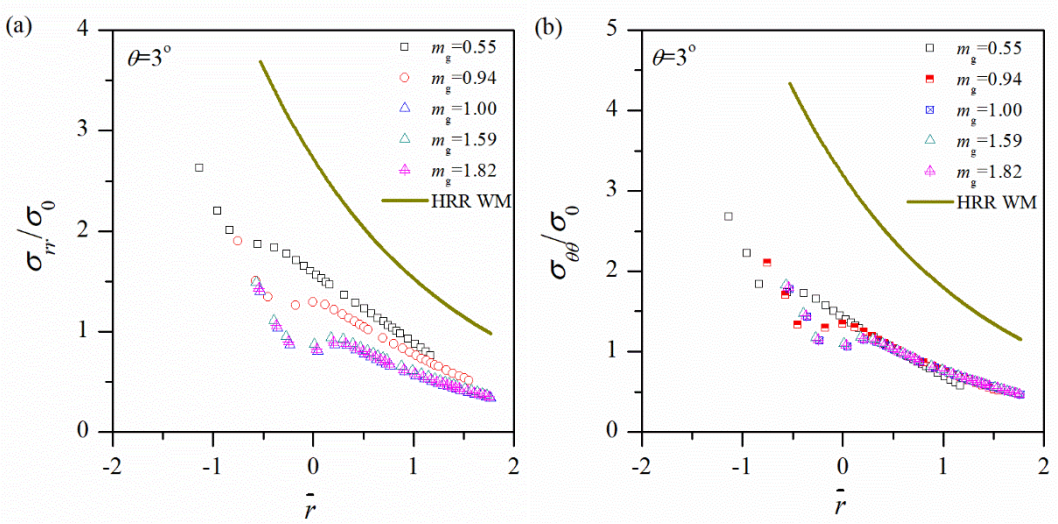

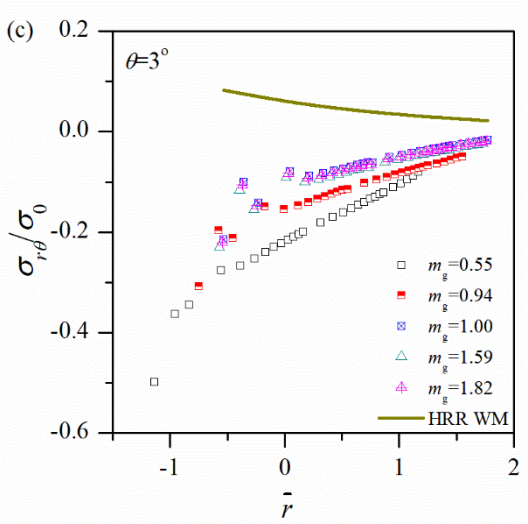

Fig. 17 Dimensionless stress distributions in radial direction along θ=3° at $t=10t_T$ under various mismatch factors for m=2.00

4.4 Material constraint characterization

It has been validated in Section 4.3 that the material mismatch will affect the interface creep crack tip field, and interface creep crack tip field presents to be self-similar property. Based on the above points and considering the similarity between interface creep crack of power-law plasticity and power-law creep, the material mismatch effect on the interface creep crack tip field can be characterized as below:

$$M^* = \frac{\sigma_{\theta\theta}^{\mathrm{M}} - \sigma_{\theta\theta}^{\mathrm{H}}}{\sigma_0} \tag{23}$$

where $\sigma_{\theta\theta}^{\mathrm{M}}$ is the opening stress which takes the material mismatch into consideration and $\sigma_{\theta\theta}^{\mathrm{H}}$ is the opening stress for the referenced stress field which does not take the material mismatch effect into account. It should be mentioned that $\sigma_{\theta\theta}^{\mathrm{H}}$ is the stress that obtained under the interface creep crack condition. It should be pointed out that the form given in Eq. (23) is very similar to that of the Q-stress presented by O'Dowd and Shih [43] as well as the elastoplastic material mismatch constraint parameter M given by Zhang et al. [45], Q_{M} proposed by Burstow et al. [38] and β_m investigated by Betegón and Peñuelas [37].

To illustrate the material constraint effect, the M^*-parameter along the $\theta=-3^o$ (in the base metal) and $\theta=3^o$ (in the weld metal) for m=0.58 are given in Fig. 18. It can be found that the values at the both sides for M^*-parameter are almost identical to each other. It implies that the selection of the reference at weld metal or base metal will not affect the difference field of mismatched case and homogeneous case. Furthermore, the M^* will decrease with the increase of the mismatch factor under m=0.58. The variations of the radial distributions for M^* under m=2.00 are given in Fig. 19. It can be found that the value of M^* under this condition is higher than zero, however, the M^* still obeys that the lower local material mismatch constraint decrease with increase of mismatch factor.

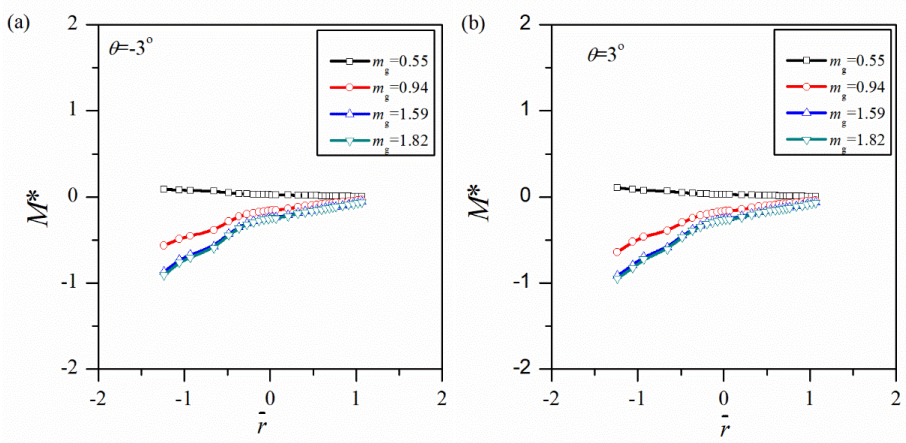

Fig. 18 Variations of the mismatch constraint effect at $t=10t_T$ under various mismatch factors along $\theta=-3^o$ and $\theta=3^o$ for m=0.58

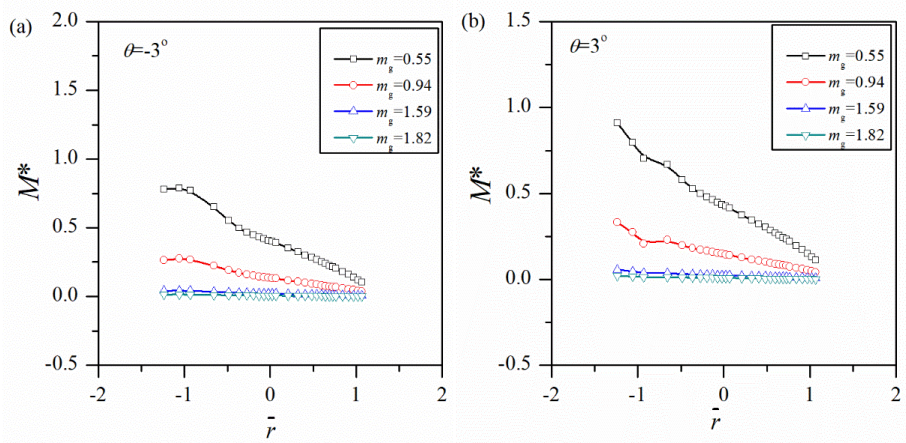

Fig. 19 Variations of the mismatch constraint effect at $t=10t_T$ under various mismatch factors along $\theta=-3^o$ and $\theta=3^o$ for m=2.00

Eq. (23) is determined by the difference field of the local mismatched one and without local mismatched one. To evaluate the M^*-parameter more clearly, an averaged

M^*-parameter for $\bar{r}$ in region of -1 and 1 are presented as below:

$$M^*_{avg} = \frac{M^*(1) - M^*(-1)}{2} \tag{24}$$

where $M^*(\pm 1)$ represents the mismatch constraint parameter calculated at $\bar{r} = 1$ and -1, respectively. With this method, M^*_{avg} under different conditions are shown in Fig. 20. M^*_{avg} decreases with the increase of mismatch factor for both m=0.58 and m=2.00 and it can be expressed as a function of mismatch factor which can be given as below:

$$M^*_{avg} = a_1 \exp^{-m/a_2} + a_3 \tag{25}$$

in which the coefficients for a_1, a_2 and a_3 are given in the following table .

Table 2 Coefficients for M^*_{avg} under different mismatch factors

m	θ(°)	a_1	a_2	a_3
0.58	+3	1.0339	0.365	-0.236
	-3	0.943	0.369	-0.192
2.00	+3	1.71	0.364	-0.00327
	-3	1.64	0.361	-0.00344

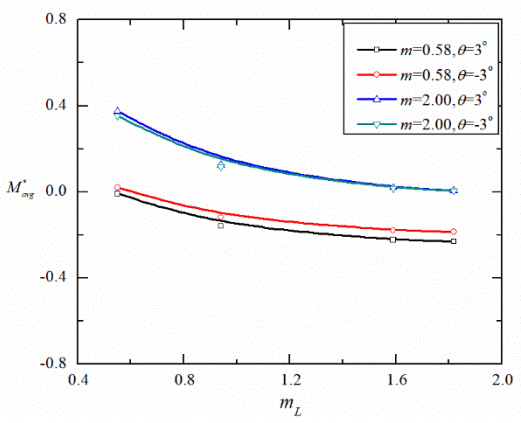

Fig. 20 Variations of the averaged M^*_{avg} with mismatch factor

4.5 Discussions on the mismatch constraint effect of M^*-field

The typical creep fracture mechanism was discussed by Lee et al. [64] and Riedel

[65]. For creep crack, three typical fracture mechanisms on microscopic view are respectively the wedge type cracking, transgranular type cracking and cavity type cracking [66]. These three type of fracture mechanisms are the functions of temperature and stress. Yagi et al. [66] found that the cavity type cracking occurs at a low gross section stress with a high temperature, and the wedge type cracking happens at high gross section stress with a lower temperature. The transgranular type cracking happens between the cavity type and the wedge type. As the material mismatch can affect the stress level, the cracking mechanism may be influenced by the mismatch effect, which needs to be further investigated. For these types of fracture at elevated temperature, the ductility decreases with the accumulation of the creep time [64]. If the creep time is long enough, the material behaves like brittle material as the creep toughness decreases with the creep time [67]. Under this condition, the proposed M^* method can be used to evaluate the stress field of interfacial creep crack on the contribution of the failure assessment diagram.

Another significant problem is the discrepancy between the dominances of the Q-term and M^*-term. The Q-term [26, 43] is strongly dependent on the applied loading level and specimen geometry size. The dominance of M^* is determined by the difference stress field caused by material mismatch. In fact, the explanations on the Q-term and the M^*-term are similar to those for elastoplastic materials with J-Q-M theory [39, 45]. In creep regime, the Q-term is dependent on the loading level, the geometry size of specimen and the creep time. The origin of the Q-term comes from high order asymptotic analyses of stress field for creep crack. For a specific creep time under steady state stage, the Q-term is symmetric and fixed as the stress contour of crack tip is not changed. However, the M^*-parameter for the M^*-field is not symmetric and comes from difference field analysis of interface creep crack.

5 Concluding remarks

Based on the investigations of the C^*-integral, stress distributions and creep zone

ahead of interface creep crack, the interface creep crack tip field is demonstrated to be self-similar under mismatch condition. With this demonstration, the material mismatch effect on the interface creep crack is studied. The detailed conclusions are drawn as below:

1) For the interface creep crack, the stress field is validated to be dependent on the strong material mismatch which make the creep crack growth to be faster at both transient and extensive creep. The under match case is found to be close to HRR field if it is evaluated with pure base metal and the over match case is nearly identical to the HRR field by estimation with pure weld metal material.
2) Compared with the general mismatched case, the local mismatch effect influence the interface creep crack tip field more significantly. The local mismatch effect influenced interface creep crack is still found to resemble the HRR type crack tip field and its stress field is also demonstrated to be self-similar.
3) The M^*-parameter is presented to characterize the material mismatch constraint effect. This proposed parameter is similar to the definition of Q-stress. The physical meaning to present the M^*-parameter is also discussed and proposed. For the extensive creep, M^*-parameter is only caused by material mismatch as the mismatch field is not changed.
4) An averaged material mismatch constraint parameter M^*_{avg} is proposed. Results show that the M^*_{avg} decreases with the increase of local material mismatch factor regardless of the general mismatch factor. M^*_{avg} could be perhaps very helpful for the characterization of the material mismatch on the interface creep crack tip field.

The work presented in this paper will further promote the understanding of the behavior of material mismatch effect on the interface creep crack. The method given in present paper will show the interface creep crack tip field in a novel perspective.

Acknowledgement

The authors acknowledge the supports from the National Natural Science Foundation of China (11902009), and the Scientific Research Common Program of Beijing Municipal Commission of Education (KM202010005034).

References

[1] Lepore, M. A., Maligno, A. R., Berto, F. 2021. A unified approach to simulate the creep-fatigue crack growth in P91 steel at elevated temperature under SSY and SSC conditions. Engineering Failure Analysis, 105569.

[2] Song M., Sun C., Zhang X., Yu H., Sun Y., Liu K., Xu T. 2021. The test on the inhomogeneous strain field and creep rupture behavior of the weld joint at elevated temperature by digital image correlation method. Engineering Failure Analysis, 120, 104997.

[3] Viespoli, L. M., Bressan, S., Itoh, T., Hiyoshi, N., Prashanth, K. G., Berto, F. 2020. Creep and high temperature fatigue performance of as build selective laser melted Ti-based 6Al-4V titanium alloy. Engineering Failure Analysis, 111, 104477.

[4] Jordan, P., Maharaj, C. 2020. Asset management strategy for HAZ cracking caused by sigma-phase and creep embrittlement in 304H stainless steel piping. Engineering Failure Analysis, 110, 104452.

[5] Huo J., Sun D., Wu H., Wang W. 2019. Multi-axis low-cycle creep/fatigue life prediction of high-pressure turbine blades based on a new critical plane damage parameter. Engineering Failure Analysis, 106, 104159.

[6] Li W., Chen H., Huang W., Chen J., Li C., Xu D., Yang H. 2021. High-temperature creep property and life prediction of aluminized AISI 321 stainless steel after annealing diffusion treatment. Engineering Failure Analysis, 128, 105611.

[7] Torabi A.R., Kalantari M. H., Aliha M. R. M., Ghoreishi S. M. N. (2019). Pure mode II fracture analysis of dissimilar Al-Al and Al-Cu friction stir welded joints using the generalized MTS criterion. Theoretical and Applied Fracture Mechanics, 104, 102369.

[8] Aliha M.R.M., Kalantari M.H., Ghoreishi S.M.N., Torabi A. R., Etesam S. (2019). Mixed mode I/II crack growth investigation for bi-metal FSW aluminum alloy AA7075-T6/pure copper joints. Theoretical and Applied Fracture Mechanics, 103, 102243.

[9] Aliha M. R. M., Ghoreishi S. M. N., Imani D. M., Fotoohi Y., Berto F. (2020). Mechanical and fracture properties of aluminium cylinders manufactured by orbital friction stir welding. Fatigue & Fracture of Engineering Materials & Structures, 43(7), 1514-1528.

[10] Xuan, F.-Z., Tu, S.-T., Wang, Z., 2004. C* estimation for cracks in mismatched welds and finite element validation. International Journal of Fracture 126, 267-280.

[11] Yang, B., Xuan, F. Z. 2018. Creep behavior of subzones in a CrMoV weldment characterized by the in-situ creep test with miniature specimens. Materials Science and Engineering: A, 723, 148-156.

[12] Zhang, W., Wang, X., Wang, Y., Yu, X., Gao, Y., Feng, Z. 2020. Type IV failure in weldment of creep resistant ferritic alloys: II. Creep fracture and lifetime prediction. Journal of the Mechanics and Physics of Solids, 134, 103775.

[13] Zerbst, U., Ainsworth, R.A., Beier, H.T., Pisarski, H., Zhang, Z.L., Nikbin, K., Nitschke-Pagel, T., Münstermann, S., Kucharczyk, P., Klingbeil, D., 2014. Review on fracture and crack propagation in weldments – A fracture mechanics perspective. Engineering Fracture Mechanics 132, 200-276.

[14] Tu, S.-T., Yoon, K.-B., 1999. The influence of material mismatch on the evaluation of time-dependent fracture mechanics parameters. Engineering Fracture Mechanics 64, 765-780.

[15] Yoon, K., Kim, K., 1999. High temperature fracture parameter for a weld interface crack. Theoretical and Applied Fracture Mechanics 32, 27-35.

[16] Wang, G.Z., Liu, X.L., Xuan, F.Z., Tu, S.T., 2010. Effect of constraint induced by crack depth on creep crack-tip stress field in CT specimens. International Journal of Solids and Structures 47, 51-57.

[17] Kitamura, T., Ngampungpis, K., Hirakata, H., 2007. Stress field near interface edge of elastic-creep bi-material. Engineering Fracture Mechanics 74, 1637-1648.

[18] Ngampungpis, K., Kitamura, T., Hirakata, H., 2007. Effect of Material Thickness on the Singular Stress Field in Elastic-creep Bi-material Interface. Journal of Solid Mechanics and Materials Engineering 1, 744-754.

[19] Ngampungpis, K., Kitamura, T., Hirakata, H., 2008. Increase of stress intensity near interface edge of elastic-creep Bi-material under a sustained load. Engineering Fracture Mechanics 75, 1285-1293.

[20] Yuan, F.G., Yang, S., 2000. Crack-tip fields for matrix cracks between dissimilar elastic and creeping materials. International Journal of Fracture 103, 327-360.

[21] Biner, S.B., 1997. A numerical analysis of time dependent stress fields ahead of stationary interface cracks at creep regime—Part I. Interface cracks in bimaterials. Engineering Fracture Mechanics 56, 513-529.

[22] Biner, S.B., 1997. A numerical analysis of time dependent stress fields ahead of stationary interface cracks at creep regime—Part II. Interface cracks in layered materials. Engineering Fracture Mechanics 56, 657-674.

[23] Yang, J., Wang, G., Xuan, F., Tu, S., 2014. Unified correlation of in-plane and out-of-plane constraint with fracture resistance of a dissimilar metal welded joint. Engineering Fracture Mechanics 115, 296-307.

[24] Yang, J., Wang, G., Xuan, F., Tu, S., Liu, C., 2014. Out-of-plane constraint effect on local fracture resistance of a dissimilar metal welded joint. Materials & Design 55, 542-550.

[25] Yamamoto, M., Miura, N., Ogata, T., 2009. Effect of constraint on creep crack propagation of mod. 9Cr-1Mo steel weld joint, ASME 2009 Pressure Vessels and Piping Conference. American Society of Mechanical Engineers, pp. 1533-1539.

[26] Dai, Y., Liu, D., Liu, Y., 2016. Mismatch constraint effect of creep crack with modified boundary layer model. Journal of Applied Mechanics 83, 031008.

[27] Hutchinson, J., 1968. Singular behaviour at the end of a tensile crack in a hardening material. Journal of the Mechanics and Physics of Solids 16, 13-31.

[28] Rice, J., Rosengren, G., 1968. Plane strain deformation near a crack tip in a power-law hardening material. Journal of the Mechanics and Physics of Solids 16, 1-12.

[29] Budden, P.J., Ainsworth, R.A., 1999. The effect of constraint on creep fracture assessments. International Journal of Fracture 97, 237-247.

[30] Chao, Y., Zhu, X., Zhang, L., 2001. Higher-order asymptotic crack-tip fields in a power-law creeping material. International Journal of Solids and Structures 38, 3853-3875.

[31] Ma, H.S., Wang, G.Z., Xuan, F.Z., Tu, S.T., 2015. Unified characterization of in-plane and out-of-plane creep constraint based on crack-tip equivalent creep strain. Engineering Fracture Mechanics 142, 1-20.

[32] Nikbin, K., 2004. Justification for meso-scale modelling in quantifying constraint during creep crack growth. Materials Science and Engineering: A 365, 107-113.

[33] Dai, Y., Liu, Y., Chao, Y. J. 2017. Higher order asymptotic analysis of crack tip fields under mode II creeping conditions. International Journal of Solids and Structures, 125, 89-107.

[34] Cui, P., Guo, W. 2020. Higher order C (t)-Tz-AT solution for three-dimensional creep crack border fields. Engineering Fracture Mechanics, 236, 107203.

[35] Tang, L.Q., Li, Y.D., Liu, C.H., 2004. Asymptotic analysis of mode II stationary growth crack on elastic-elastic power law creeping bimaterial interface. Applied Mathematics and Mechanics 25, 228-235.

[36] Hui, C.-Y., Saif, M., 1994. Asymptotic stress field of a mode III crack growing along an elastic/elastic power-law creeping bimaterial interface. Journal of Applied Mechanics 61, 384-389.

[37] Betegón, C., Peñuelas, I., 2006. A constraint based parameter for quantifying the crack tip stress fields in welded joints. Engineering Fracture Mechanics 73, 1865-1877.

[38] Burstow, M.C., Howard, I.C., Ainsworth, R.A., 1998. The influence of constraint on crack tip stress fields in strength mismatched welded joints. Journal of the Mechanics and Physics of Solids 46, 845-872.

[39] Thaulow, C., Zhang, Z., Hauge, M., 1997. Effects of crack size and weld metal mismatch on the cleavage toughness of wide plates. Engineering Fracrure Mechanics 57, 653-664.

[40] Hoff, N., 1954. Approximate analysis of structures in the presence of moderately large creep deformations. Quarterly of Applied Mathematics 12, 49.

[41] Shih, C.F., Asaro, R.J., 1988. Elastic-Plastic Analysis of Cracks on Bimaterial Interfaces: Part I—Small Scale Yielding. Journal of Applied Mechanics 55, 299-316.

[42] Shih, C.F., Asaro, R.J., 1989. Elastic-Plastic Analysis of Cracks on Bimaterial Interfaces: Part II—Structure of Small-Scale Yielding Fields. Journal of Applied Mechanics 56, 763-779.

[43] Shih, C.F., Asaro, R.J., O'Dowd, N.P., 1991. Elastic-Plastic Analysis of Cracks on Bimaterial Interfaces: Part III—Large-Scale Yielding. Journal of Applied Mechanics 58, 450-463.

[44] Wang, T.C., 1990. Elastic-plastic asymptotic fields for cracks on bimaterial interfaces. Engineering Fracture Mechanics 37, 527-538.

[45] Zhang, Z., Hauge, M., Thaulow, C., 1996. Two-parameter characterization of the near-tip stress fields for a bi-material elastic-plastic interface crack. International Journal of Fracture 79, 65-83.

[46] O'Dowd, N.P., Shih, C.F., 1992b. Family of crack-tip fields characterized by a triaxiality parameter—II. Fracture applications. Journal of the Mechanics and Physics of Solids 40, 939-963.

[47] Yang, S., Chao, Y.J., Sutton, M.A., 1993. Higher order asymptotic crack tip fields in a power-law hardening material. Engineering Fracture Mechanics 45, 1-20.

[48] Østby, E., Zhang, Z., Thaulow, C., 2001. Constraint effect on the near tip stress fields due to difference in plastic work hardening for bi-material interface cracks in small scale yielding. International Journal of Fracture 111, 87-103.

[49] Lee, H., Kim, Y.-J., 2001. Interfacial crack-tip constraints and J-integrals in plastically mismatched bi-materials. Engineering Fracture Mechanics 68, 1013-1031.

[50] Matvienko, Y.G., Shlyannikov, V., Boychenko, N., 2013. In-plane and out-of-plane constraint parameters along a three-dimensional crack-front stress field under creep loading. Fatigue & Fracture of Engineering Materials & Structures 36, 14-24.

[51] Shlyannikov, V., Boychenko, N., Tartygasheva, A., 2011. In-plane and out-of-plane crack-tip constraint effects under biaxial nonlinear deformation. Engineering Fracture Mechanics 78, 1771-1783.

[52] Dai Y., Qin F., Liu Y., Berto F., Chen H. 2021. Characterizations of material constraint effect for creep crack in center weldment under biaxial loading. International Journal of Fracture, 1-17.

[53] Rice, J.R., Suo, Z., Wang, J.-S., 1990. Mechanics and thermodynamics of brittle interfacial failure in bimaterial systems.

[54] Hibbitt, Karlsson, Sorensen, 2011. ABAQUS User's Manual, Version 6.10.

[55] Dehghany M., Saeidi Googarchin H., Aliha M.R.M. (2017). The role of first non-singular stress terms in mixed mode brittle fracture of V-notched components: An experimental study. Fatigue & Fracture of Engineering Materials & Structures, 40(4), 623-641.

[56] Ayatollahi M. R., Nejati, M. (2011). Determination of NSIFs and coefficients of higher order terms for sharp notches using finite element method. International Journal of Mechanical Sciences, 53(3), 164-177.

[57] Han J.-J., Lee K.H., Kim, Y.J., Nikbin K., Dean D., 2011. Effects of geometry and combined loading on steady-state creep stresses in welded branches. International Journal of Pressure Vessels and Piping 88, 395-402.

[58] Bassani, J., McClintock, F., 1981. Creep relaxation of stress around a crack tip. International Journal of Solids and Structures 17, 479-492.

[59] Li, F.Z., Needleman, A., Shih, C.F., 1988. Characterization of near tip stress and deformation fields in creeping solids. International Journal of Fracture 36, 163-186.

[60] Riedel, Rice, 1980. Tensile cracks in creeping solids. West Conshohocken, PA: ASTM STP 700, 112-130.

[61] Al Laham, S., Branch, S.I., Ainsworth, R., 1998. Stress intensity factor and limit load handbook. British Energy Generation Limited.

[62] Shlyannikov, V.N., Tumanov, A.V., Boychenko, N.V., 2015. A creep stress intensity factor approach to creep–fatigue crack growth. Engineering Fracture Mechanics 142, 201-219.

[63] Dai, Y., Qin, F., Liu, Y., Chao, Y. J. 2021. On the second order term asymptotic solution for sharp V-notch tip field in elasto-viscoplastic solids. International Journal of Solids and Structures, 217, 106-122.

[64] Lee, J.S., Armaki, H.G., Maruyama, K., Muraki, T., Asahi, H., 2006. Causes of breakdown of creep strength in 9Cr–1.8W–0.5Mo–VNb steel. Materials Science and Engineering: A 428, 270-275.

[65] Riedel, H., 1987. Fracture at high temperatures. Springer.

[66] Yagi, K., Tabuchi, M., Kubo, K., Jong Jip, K., Yong Hak, H., 1997. The influence of fracture

mechanisms on the creep crack growth behavior of 316 stainless steel. Engineering Fracture Mechanics 57, 463-473.

[67] Davies, C.M., 2009. Predicting creep crack initiation in austenitic and ferritic steels using the creep toughness parameter and time-dependent failure assessment diagram. Fatigue & Fracture of Engineering Materials & Structures 32, 820-836.

Table and caption figures

Table 1 Material constants used in calculations with the same creep exponent

Table 2 Coefficients for M_{avg}^{*} under different mismatch factors

Fig. 1 Coordinate system for interface crack tip

Fig. 2 The configurations and FE meshes of (a) SECP and (b) MBLM as well as crack tips

Fig. 3 Variation of $C(t)$-integral with creep time under different mismatch factors for (a) MBLM and (b) SECP

Fig. 4 Variation of $C(t)$-integral with normalized creep time

Fig. 5 Isoline of equivalent creep strain with level of 0.2% for interface creep crack with different mismatch factors at $t=10t_{\mathrm{T}}$

Fig. 6 Isoline of equivalent creep strain with level of 0.2% for m=0.58 considering mismatch effect at $t=10t_{\mathrm{T}}$

Fig. 7 Isoline of equivalent creep strain with level of 0.2% for m=2.00 considering mismatch effect at $t=10t_{\mathrm{T}}$

Fig. 8 Comparisons of angular stress distributions for MBLM with different mismatch factors

Fig. 9 Angular distributions of interface creep crack tip for (a) radial stress, (b) tangential stress and (c) shearing stress

Fig. 10 Comparisons of angular stress distributions for SECP with different mismatch factors

Fig. 11 Normalized radial stress distributions along $\theta=3^{\mathrm{o}}$: (a), (b) and $\theta=-3^{\mathrm{o}}$: (c), (d)

Fig. 12 Dimensionless angular stress distributions at $t=10t_{\mathrm{T}}$ under various mismatch factors for general mismatch factor m=0.58

Fig. 13 Dimensionless stress distributions in radial direction along θ=-3$^{\mathrm{o}}$ under various mismatch factors for m=0.58

Fig. 14 Dimensionless stress distributions in radial direction along θ=3$^{\mathrm{o}}$ at $t=10t_{\mathrm{T}}$ under various mismatch factors for general mismatch factor m=0.58

Fig. 15 Dimensionless angular stress distributions at $t=10t_{\mathrm{T}}$ under various mismatch factors for m=2.00

Fig. 16 Dimensionless stress distributions in radial direction along θ=-3$^{\mathrm{o}}$ at $t=10t_{\mathrm{T}}$ under various mismatch factors for m=2.00

Fig. 17 Dimensionless stress distributions in radial direction along θ=3$^{\mathrm{o}}$ at $t=10t_{\mathrm{T}}$ under various mismatch factors for m=2.00

Fig. 18 Variations of the mismatch constraint effect at $t=10t_{\mathrm{T}}$ under various mismatch factors

along $\theta = -3^{\circ}$ and $\theta = 3^{\circ}$ for m=0.58

Fig. 19 Variations of the mismatch constraint effect at $t = 10t_{\mathrm{T}}$ under various mismatch factors along $\theta = -3^{\circ}$ and $\theta = 3^{\circ}$ for m=2.00

Fig. 20 Variations of the averaged M^{*}_{avg} with mismatch factor